IEEE Access
Multidisciplinary | Rapid Review | Open Access Journal

Received October 24, 2021, accepted October 29, 2021, date of publication November 2, 2021, date of current version November 11, 2021.

Digital Object Identifier 10.1109/ACCESS.2021.3124903

A Novel Framework for Centrifugal Pump Fault Diagnosis by Selecting Fault Characteristic Coefficients of Walsh Transform and Cosine Linear Discriminant Analysis

ZAHOOR AHMAD[1], AKHAND RAI[1,2], MD JUNAYED HASAN[1], CHEOL HONG KIM[3], AND JONG-MYON KIM[1,4], (Member, IEEE)

[1]Department of Electrical, Electronics, and Computer Engineering, University of Ulsan, Ulsan 44610, South Korea
[2]School of Engineering and Applied Science, Ahmedabad University, Ahmedabad, Gujarat 380009, India
[3]School of Computer Science and Engineering, Soongsil University, Seoul 06978, South Korea
[4]PD Technology Cooperation, Ulsan 44610, South Korea

Corresponding author: Jong-Myon Kim (jmkim07@ulsan.ac.kr)

This work was supported in part by the Korea Institute of Energy Technology Evaluation and Planning (KETEP), and in part by the Ministry of Trade, Industry & Energy (MOTIE) of the Republic of Korea under Grant 20192510102510.

ABSTRACT In this paper, we propose a three-stage lightweight framework for centrifugal pump fault diagnosis. First, the centrifugal pump vibration signatures are fast transformed using a Walsh transform, and Walsh spectra are obtained. To overcome the hefty noise produced by macro-structural vibration, the proposed method selects the fault characteristic coefficients of the Walsh spectrum. In the second stage, statistical features in the time and Walsh spectrum domain are extracted from the selected fault characteristic coefficients of the Walsh transform. These extracted raw statistical features result in a hybrid high-dimensional space. Not all these extracted features help illustrate the condition of the centrifugal pump. To overcome this issue, novel cosine linear discriminant analysis is introduced in the third stage. Cosine linear discriminant analysis is a dimensionality reduction technique which selects similar interclass features and adds them to the illustrative feature pool, which contains key discriminant features that represent the condition of the centrifugal pump. To achieve maximum between-class separation, linear discriminant analysis is then applied to the illustrative feature pool. This combination of illustrative feature pool creation and linear discriminant analysis forms the proposed application of cosine linear discriminant analysis. The reduced discriminant feature set obtained from cosine linear discriminant analysis is then given as an input to the K-nearest neighbor classifier for classification. The classification results obtained from the proposed method outperform the previously presented state-of-the-art methods in terms of fault classification accuracy.

INDEX TERMS Centrifugal pump, cosine linear discriminant analysis, fault diagnosis, walsh transform.

I. INTRODUCTION

Centrifugal pumps (CPs) perform essential tasks in many industrial processes. In 2017, a study was conducted on the failure of 437 CPs that showed that 6128 hours were spent on CP maintenance with a cost of 50 million dollars due to the lack of predictive maintenance [1]. Despite the time and economic losses, performance degradation also poses serious safety hazards [2]. Early fault diagnosis of CP is of primary importance to overcome the time consumption, economic losses, and safety hazards due to CP performance degradation.

Performance degradation in a CP can be caused either by mechanical faults (MF) or fluid flow-related hydraulic faults [3]. Specifically, 34% of MFs in the CP are related to mechanical seal faults [4]. Furthermore, impeller defects in the CP can cause both mechanical and hydraulic faults in the CP [5]. Additionally, MFs can cause either soft or hard failure in the CP. Hard failures are dangerous, but they are easy to identify. In the case of soft failure, the CP performance degrades slowly, requiring an intelligent method for fault identification [6]. For this reason, this study focuses on soft

The associate editor coordinating the review of this manuscript and approving it for publication was Shen Yin.

This work is licensed under a Creative Commons Attribution 4.0 License. For more information, see https://creativecommons.org/licenses/by/4.0/

failure related to MFs, specifically due to mechanical seal scratches (MSS), mechanical seal holes (MSH), and faults due to impeller defects.

A MF in the CP affects the stiffness of the mechanical specimen, and this change in the stiffness produces an impulse or variation in the vibration signatures [7], [8]. Therefore, vibration signals (VS) can be efficiently used for the CP fault diagnosis [9]. These variations in the vibration signatures change the amplitude of the impulses in the Fourier spectrum at a specific fault characteristic frequency (FCF) [10]. However, these fault characteristic impulses (FCI) are often overwhelmed by impulsive noise and unnecessary macrostructural vibration noise because of their low energy content [11]. Furthermore, The complex fluid and mechanical interaction inside the pump and the variation in vibration signal due to the stiffness change of the mechanical components make the statistical properties of the vibration signal vary with time. thus the signal becomes nonlinear and non-stationary and it is known that sinusoidal transforms, such as Fourier transforms are not effective in the case of non-stationary signals [12]. Multi-band envelop detection has been widely used to detect the FCIs in the vibration signatures [13]. However, a narrow band signal demodulation technique suffers from being unable to distinguish between interference impulses and FCIs. To overcome this issue, Tra and Kim [14] used the blind source separation (BSS) technique for acoustic emission signal denoising. Furthermore, Antoni [15], [16] introduced spectral kurtosis and a fast kurtogram as an indicator for selecting optimal frequency bands for FCIs. However, the BSS technique needs a baseline signal to ensure noise reduction in the resulting signal. On the other hand, spectral kurtosis is sensitive to periodic noises because of its primary focus on the impulsiveness of the signal. When applied to non-stationary VS, wavelet transform (WT) has remarkable advantages because WT is sensitive for longer duration defects reflected by non-stationary impulses [17]–[19]. Unfortunately, WT also has some drawbacks. For example, WT suffers from the oscillation effects when an inappropriate mother wavelet is selected for decomposition [20]. An adaptive signal decomposition method called empirical mode decomposition (EMD) was introduced to overcome the shortcomings of WT [21]. However, EMD suffers from mode mixing, extreme interpolation, distortion of faulty impulses and its limited mathematical background, making it less attractive over WT [22]. Different from sinusoidal-type transforms, specifically non-sinusoidal type transforms such as Walsh transforms are appropriate for the impulsive signals and can be used to overcome the limitations of the sinusoidal-type transforms [23]. Furthermore, Walsh transforms have no multipliers and can transform a complicated impulse signal into rectangular waveforms called Walsh coefficients with smaller computational complexity [24]. To reduce the noise, higher coefficients are truncated as the signal energy is concentrated at lower coefficients of the Walsh transform [25]. However, due to the orthogonality property of the Rademacher function used in the Walsh transform, truncating higher coefficients without predetermining the fault characteristic coefficients can cause important fault-related FCIs loss. In the case of CPs (which involve complex mechanical components and fluid interactions), focusing just on the lower coefficients of the Walsh transform is not a convenient choice. Therefore, in this study, a new, fast CP fault diagnosis method based on Walsh Transform was developed. For signal preprocessing, the new fault diagnosis strategy first defines fault characteristic modes of vibration (MOV) where the FCIs of CP can be perceived. Furthermore, to overcome the macrostructural vibration noise and the truncating issue of the Walsh transform, the fault characteristic coefficients of the Walsh transform will be identified and selected for fault feature extraction.

Fault detection and diagnosis based on intelligence methods consist of signal statistical indicator extraction, preprocessing of the statistical features, and classification of faults [26]–[28]. Feature extraction from the VS is the most important step in intelligent fault diagnosis. Herein, statistical indicators from the VS are extracted in the time, frequency, and time-frequency domain [29]. However, these raw statistical features are not appropriate for incipient faults and are also not sensitive to severe faults and can affect the fault classification accuracy [30]. Furthermore, a high-dimensional feature vector is created when all these features are combined into a single feature vector. However, all the features do not illustrate the class discriminatory information, making it important to extract the intrinsic information and to enhance the classification accuracy [31]. In the past, numerous dimensionality reduction and feature evaluation techniques have been proposed. Linear discriminant analysis (LDA) and principal component analysis (PCA) are the prominent ones among them [32]. Sakthivel *et al.* [33] conducted a comparative study between dimensionality reduction and feature classification techniques and found that PCA performs better for CP fault classification. PCA considers variance in the feature and uses this information to construct a low-dimensional representation of the features. However, the selection of principal components leads to information losses. Furthermore, PCA does not consider the between-class separability. In contrast, LDA considers the inter-class scatteredness and between-classes separability for low-dimensional representation of the features. Several variants of LDA such as sensitive discriminant analysis, trace ratio LDA, and robust linear optimized LDA have been proposed in the past decade [34]–[37]. However, the between-class separation represented by the penalty graph can affect the fault classification accuracy. To address this issue, analyzing the hidden patterns in the raw statistical features before applying LDA is of main importance. In this paper, we propose a new technique called cosine LDA. Cosine LDA first selects highly illustrative features in each class and adds them to the illustrative feature pool. The LDA is applied to the illustrative feature pool to maintain original class information and to increase between-class separation. This combination of illustrative feature pool formation and LDA forms the core of cosine LDA. The contributions

of this paper can be summarized into the following three aspects.

1. A new, fast CP fault diagnosis method based on Walsh Transform has been proposed in this paper. The new fault diagnosis strategy first defines fault characteristic modes of vibration (MOV) where the Fault characteristic impulses of CP can be perceived. Furthermore, to overcome the macrostructural vibration noise and the truncating issue of the Walsh transform, the Walsh coefficients of the fault characteristic MOV will be selected for fault feature extraction. To the best of our knowledge, selecting fault characteristic coefficients of the Walsh transform based on fault characteristic MOV for CP fault diagnosis has not been reported in the past.
2. Cosine LDA is proposed for CP mechanical fault diagnosis. To the best of our knowledge, preprocessing features using Cosine LDA has not been reported in the past. Cosine LDA first selects highly illustrative features in each class and adds them to the illustrative feature pool. To maintain original class information and to increase between-classes separation, the LDA matrices are applied to the illustrative feature pool.
3. Real CP mechanical fault vibration data is used to validate the effectiveness of the proposed method for CP mechanical fault diagnosis.

The rest of the study is arranged as follows. The technical background of Walsh transforms and LDA is presented in Section 2. The data collection and experimental setup are explained in Section 3. Section 4 introduces the proposed CP mechanical fault diagnosis method. The experimental results and comparison of the proposed method with other state-of-the-art methods are presented in Section 5. Section 6 presents the concluding remarks, along with future research directions.

II. TECHNICAL BACKGROUND

A. REVIEW OF WALSH TRANSFORM

The definition for the Walsh function changes according to the targeted application domain. That is, strict sequence ordering Walsh function is appropriate for communication purposes, while the Hadamard function is applicable for control applications. The Rademacher function is appropriate for signal processing. Thus, the Walsh transform can be derived from the Rademacher function for signal processing.

$$r(l+1,x) = Sign(\sin 2\pi 2^l x), \quad \text{where,} \quad l = 0, 1, \ldots, L;\ 0 \le x < 1, \tag{1}$$

Equation (1) represents the Rademacher function where $r(0,x) = 1, N$ is the signal data points. The $Sign(y)$ is expressed in (2).

$$Sign(y) = \begin{cases} +1, & y \le 0 \\ -1, & y < 0. \end{cases} \tag{2}$$

The Walsh function $\Phi(n,t)$ can be expressed in terms of the product of the Rademacher function as in (3).

$$\Phi(n,t) = \prod_{i=1}^{N} r(i+1,t)^{n_i}, \quad n_i \in \{0,1\}, \tag{3}$$

A signal $f(t)$ can be represented in terms of the Walsh series as follows:

$$f(t) = \sum_{n=0}^{N-1} A_n \Phi(n,t), \tag{4}$$

Here, A_n expresses Walsh coefficients in (4). The Walsh coefficients for a signal $f(t)$ having length N can be represented by:

$$A_n = \frac{1}{N} \sum_{n=0}^{N-1} f_n \Phi(n,t), \tag{5}$$

Equation (5) reveals that the base vector representing Walsh coefficients consists of the values '−1' or '+1'. Furthermore, there is no use of complex numbers, and the transform is based on simple arithmetic operations of real numbers. This makes the Walsh transform computationally fast compared to other non-sinusoidal transforms.

B. REVIEW OF LDA FOR MULTI-CLASS

The LDA is a supervised dimensionality reduction algorithm that preserves original class information while projecting the data of a high dimension into a lower dimension space. The optimal class discrimination matrix is obtained by minimizing the within-class scatteredness and maximizing between-class distance. In multiclass LDA, the within-class scatter matrix and between-classes distance matrix can be represented as follows:

$$I_s = \sum_{j=1}^{J} I_j^2 = \sum_{j=1}^{J} \sum_{\mathrm{m}_i \in class_i} (m_i - \mu_i) - (m_i - \mu_i)^t, \tag{6}$$

where m_i is the feature and μ_i is the mean of $class_i$ in (6).

$$C_s = \sum_{j=1}^{J} n_j (\mu_j - \mu)(\mu_j - \mu)^t \tag{7}$$

$$\text{where } \mu = \frac{1}{N} \sum_{j=1}^{J} n_j \mu_j. \tag{8}$$

The feature number is represented by n_j, the number of features in each class is represented by N, and the rank of between-class distance matrix C_s is *j-1* for $cluster_j$ in (7). Assume that T is the transform matrix that will allow a high dimensional statistical feature space to be reduced to a low dimension space. Based on (2) and (3), the transform matrix T can be expressed as follows:

$$\tilde{I}_s = T^t I_s T \tag{9}$$

$$\tilde{C}_s = T^t C_s T. \tag{10}$$

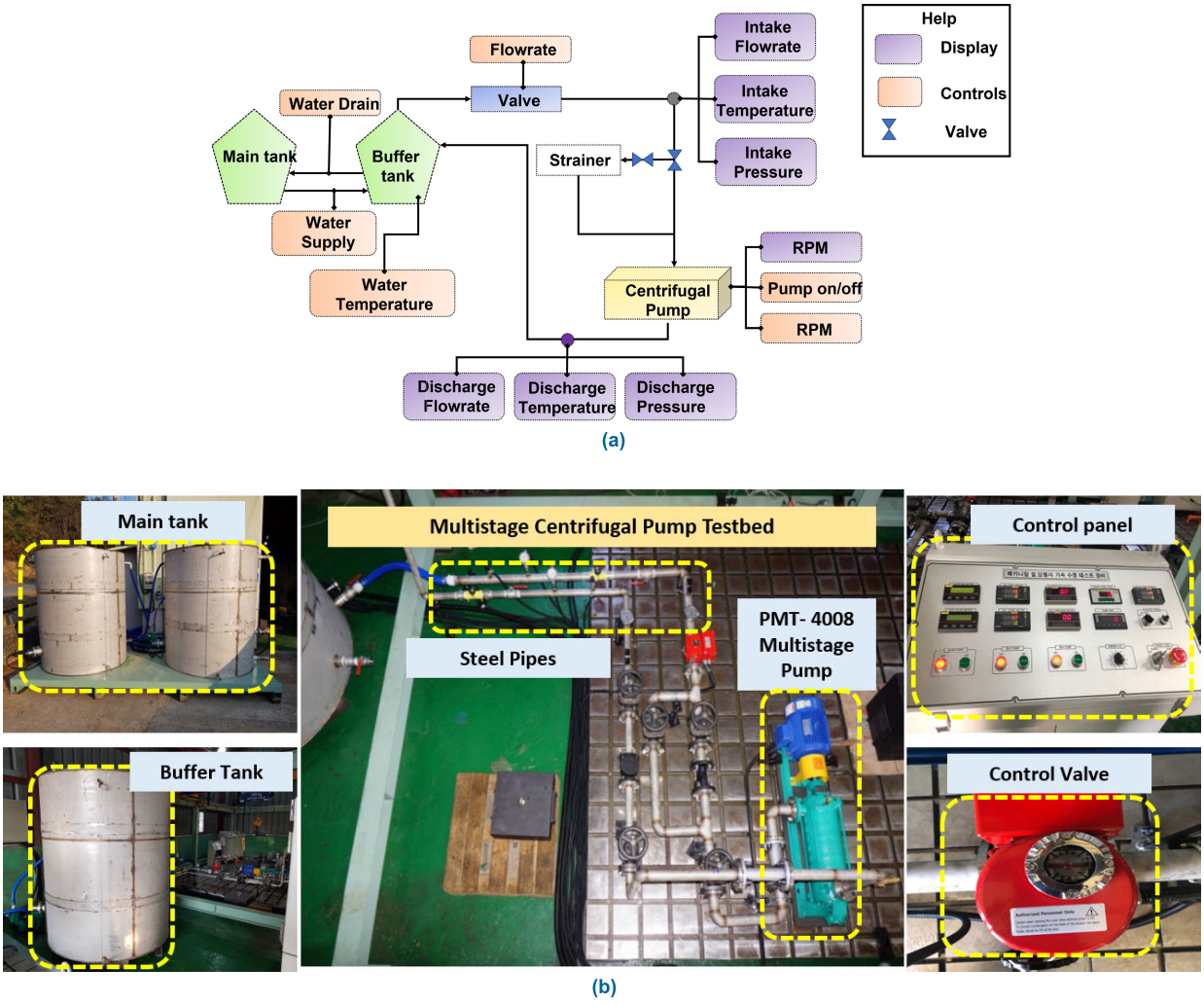


FIGURE 1. Centrifugal pump testbed for mechanical faults diagnosis (a) schematics (b) pictorial.

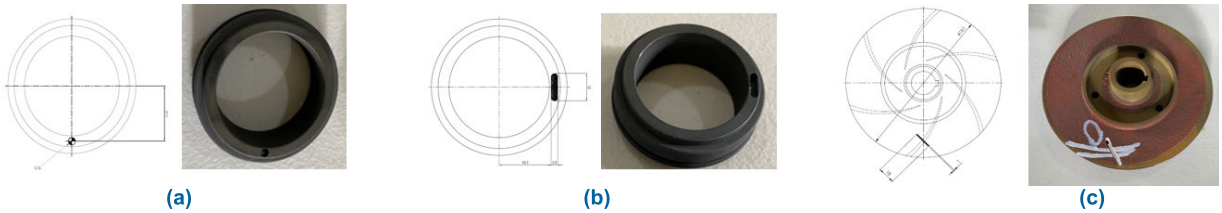


FIGURE 2. Faults created in the mechanical components of the CP (a) A hole in mechanical seal (b) A scratch in mechanical seal (c) A piece of metal removed from impeller.

In (9) and (10) $\tilde{I}_s$ is the projected within the class scatteredness, and $\tilde{C}_s$ is the discrimination matrix between classes. From (9) and (10), the objective function can be derived as (11) and (12).

$$J(T) = \frac{\det(\tilde{I}_s)}{\det(\tilde{C}_s)} \tag{11}$$

$$C_s T = \lambda I_s T, \quad \left(\lambda = \frac{T^t C_s T}{T^t I_s T}\right) \tag{12}$$

Equation (12) has at most $I - 1$ eigenvectors, and the eigenvectors are represented by the members of projection matrix T as $T_1, T_2, \ldots, T_{I-1}$ respectively. The reduced dimensional feature space is presented by the largest L eigenvalues corresponding to the linearly independent eigenvectors. Therefore, a high dimensional feature space can be projected into a reduced subspace of dimension $I - 1$ using LDA.

III. PUMP TEST RIG SETUP

A self-developed CP test rig was used for MF experiments, the test rig and its schematics are shown in Figure 1(a) and 1(b). A multistage CP PMT-4008 with

a 5.5kW electric motor was used to pump water from the main tank to the buffer tank through clear steel pipes. A separate control panel was established for controlling the electric power, speed, and flow rate of the pump. After turning on the power from the control panel, the CP was operated at a speed of 1733 rpm, and the vibration signature was recorded from the CP under different operating conditions.

Four accelerometers (622b01-accelerometer) were used to record the vibration signature from the CP. Two accelerometers were attached to the pump casing, one accelerometer was mounted near the impeller, and one was mounted near the mechanical seal. Each accelerometer uses an independent channel for recording the vibration data. The vibration data were digitized using a DAQ from National Instruments (NI-9234).

The vibration signature from the CP was recorded under normal, impeller fault (IF), MSH, and MSS conditions. In each condition, the CP was operated for 300 seconds, and a total of 1200 samples were collected from the CP at a sampling rate of 26.5kHz. A hole of 2.8mm diameter and depth of 2.8mm was seeded in the rotating part of a mechanical seal having an inner diameter of 38mm for MSH conditions as shown in Figure 2(a). For the MSS condition, a scratch was made with a diameter of 2.5mm and depth of 2.8mm in the rotating part of the mechanical seal, as shown in Figure 2(b). For the impeller defect condition, a metal piece was removed from the surface of the impeller with a length of 18mm and a depth of 2.8mm as shown in Figure 2(c). The vibration signatures of the CP obtained under normal and defective operating conditions are presented in Figure 3.

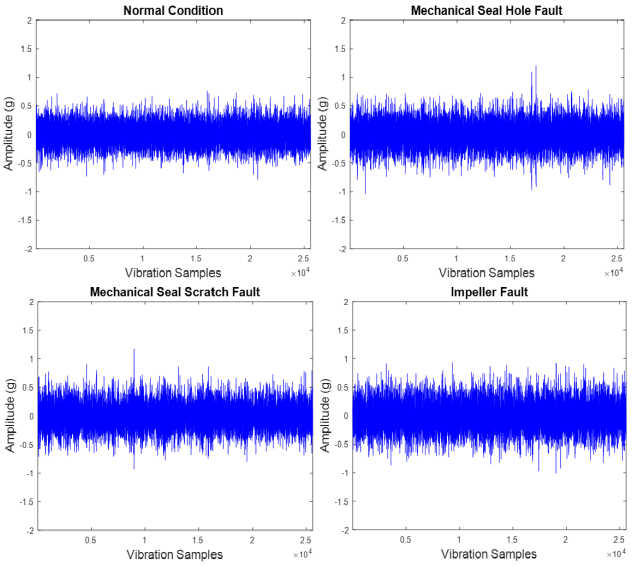


FIGURE 3. CP vibration signatures under normal and defective operating conditions.

IV. PROPOSED FAULT DIAGNOSIS FRAMEWORK

The proposed fault diagnosis framework starts with a fast transformation of the VS obtained from the CP under normal and defective operation conditions and ends with CP fault classification as shown in Figure 4. The steps involved in the proposed fault diagnosis strategy are explained in this section.

A. STEP-1: SELECTION OF THE FAULT CHARACTERISTIC COEFFICIENT OF WALSH TRANSFORM

A MF affects the stiffness of the CP mechanical components. These changes in the stiffness result in specific FCIs in the vibration spectrum of the CP. These FCIs occur at lower frequencies and contain little energy. Thus, they are overwhelmed by macrostructural vibration noise. A non-sinusoidal type of transform such as a Walsh transform can mitigate this issue as the high energy impulses occur at lower coefficients. In addition to this, identifying and selecting the fault characteristic coefficient of the Walsh transform is very important as the discriminancy of the statistical features is based on the preprocessing of the VS. For this reason, the fault characteristic coefficient of the Walsh transform is identified and selected for feature extraction in this step.

In CP, there are electronic, excitation frequencies and generated frequencies. The excitation and generated frequencies

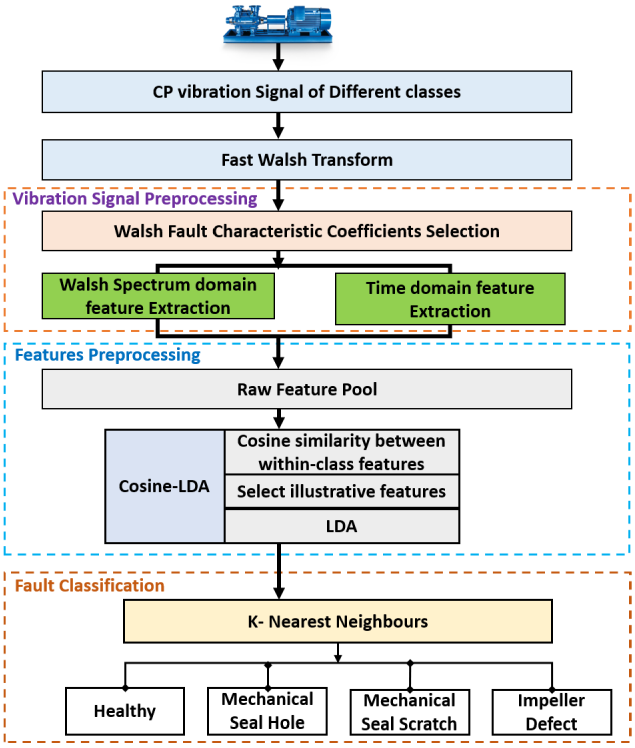


FIGURE 4. Proposed framework for centrifugal pump fault diagnosis.

are valuable frequencies for the identification of the fault characteristic coefficient of the Walsh transform. These frequencies can be identified in the vibration spectrum if the basic geometry and the speed of the CP are known.

Generated frequencies are responsible for the FCIs of IF [38]. IF appears in the frequency spectrum in the form of impeller imbalance. The impeller imbalance occurs at a specific fault characteristic frequency in the vibration spectrum

of the CP. These FCIs can be calculated using (13).

$$FCI_{i.defect} = n.R \tag{13}$$

The number of harmonics is represented by n, and the rotating speed in Hz is given by R in (13). The equation for the FCIs of IF also assures the 13373-1:2002 ISO standard for machine condition monitoring [39]. The $FCI_{i.defect}$ are calculated up to the 5th harmonic, as can be seen in Figure 5. Figure 5(a) shows the Walsh spectrum of the CP under normal conditions. Figure 5(b) shows the Walsh coefficients of the CP obtained under IF conditions. It is evident from Figure 5(b) that FCIs appear in the Walsh spectrum due to impeller defects.

CP excitation frequency in the vibration spectrum is a valuable feature for the identification of mechanical seal-related faults. A single amplified impulse present in the vibration spectrum of the CP represents the excitation frequency. In the case of mechanical seal-related faults, the excitation frequency for CP can be determined from the vibration theory of a ring.

From the vibration kinetic energy E_{KE} and deformation potential energy E_{PE}, the conservation of energy can be written as:

$$\frac{d}{dt}(E_{KE} + E_{PE}) = 0 \tag{14}$$

where

$$E_{KE} = \left(\frac{1}{2}\rho A\right)(\dot{u}^2)(2\pi r) \tag{15}$$

$$E_{PE} = \left(\frac{1}{2}(AEu^2/r^2)\right)(2\pi r). \tag{16}$$

Here, ρ is the material density, A is the cross-sectional area, radial displacement is u, E represents the elasticity modulus, and r is the ring centerline radius in (15) and (16). By solving (14) using (15) and (16), we can get the fundamental frequency as follows:

$$f_{c.ring} = \left(\frac{1}{2\pi r}\right)\sqrt{\frac{E}{\rho}} \tag{17}$$

$f_{c.ring}$ is the circular ring fundamental frequency. For complex vibratory systems, there are specific MOVs, such as torsional and flexural MOVs. In the case of a mechanical seal, the fundamental and torsional vibration have high frequencies. However, flexural vibration exists at lower frequencies. The mechanical seal natural frequency in flexural vibration and its corresponding bending MOV can be calculated using (18).

$$f_{flexural} = \left(\frac{n\left(n^2-1\right)}{\pi\, d^2\sqrt{n^2+1}}\right)\sqrt{\frac{E\,t^2}{3\rho}} \tag{18}$$

Here, d is the diameter of the ring, t is the thickness of the ring, and $n = 1, 2, \ldots, 5$ represent the MOVs. After calculating the flexural vibration and its corresponding bending modes for the mechanical seal using (18), we observed that the CP excitation frequency changes whenever a mechanical seal defect occurs as shown in Figure 6. Figure 6(a) shows the Walsh spectrum of CP under normal conditions. In contrast, Figure 6(b) shows the Walsh spectrum of CP under MSH fault. It is noticeable from Figure 6(b) that the impulse representing excitation frequency is in between the 1st and 2nd modes of flexural vibration with a slight increase in amplitude. For MSS, the impulse representing excitation frequency is in between the 2nd and 3rd modes of flexural vibration with an increase in the amplitude as can be seen in Figure 6(c).

As discussed earlier, identifying and selecting the fault characteristic coefficient of the Walsh transform is very important as the discriminancy of the statistical features is based on the preprocessing of the VS. Thus, the fault characteristic coefficient of the Walsh transform is selected up to the 3rd mode of flexural vibration for feature extraction in this step. These Walsh coefficients cover the FCIs of impeller defects and the CP excitation frequencies for normal and mechanical seal defects. In this paper these coefficients are referred to as fault characteristic coefficients of the Walsh transform.

B. STEP-2: RAW FEATURES EXTRACTION

Raw features in the spectral and spatial domain are extracted from the selected fault characteristic coefficients of the Walsh transform. A total of 16 features adapted from [26] are extracted from the preprocessed VS under each CP operating condition. All these features are combined into a single feature vector, which forms a high dimensional raw hybrid feature pool.

C. STEP-3: COSINE LINEAR DISCRIMINANT ANALYSIS

Discriminant features are very important for precise classification. The high dimensional raw hybrid feature pool might have some irrelevant features that can affect the CP condition classification. To overcome this issue, identification of the intrinsic patterns in the feature space is of greater importance. For this reason, a new feature illustration-based dimensionality reduction method called cosine LDA is introduced in this step. The various steps involved in cosine LDA are as follows:

1. Cosine similarity between feature F_i with other within the class features F_j is calculated using (19).

$$C_{sim}(F_i, F_j) = \frac{F_i.F_j}{\|F_i\|\,\|F_j\|} \tag{19}$$

2. The cosine similarity values for each feature are summed up, which results in an illustrative value I_{value} for the feature F_i.

$$I_{value} = \sum_{i=1}^{n} C_{sim} \tag{20}$$

3. If the I_{value} for a feature F_i is greater than 0, then the feature will be included in the illustrative feature pool $I_{F.pool}$. If not, it will be included in the less illustrative

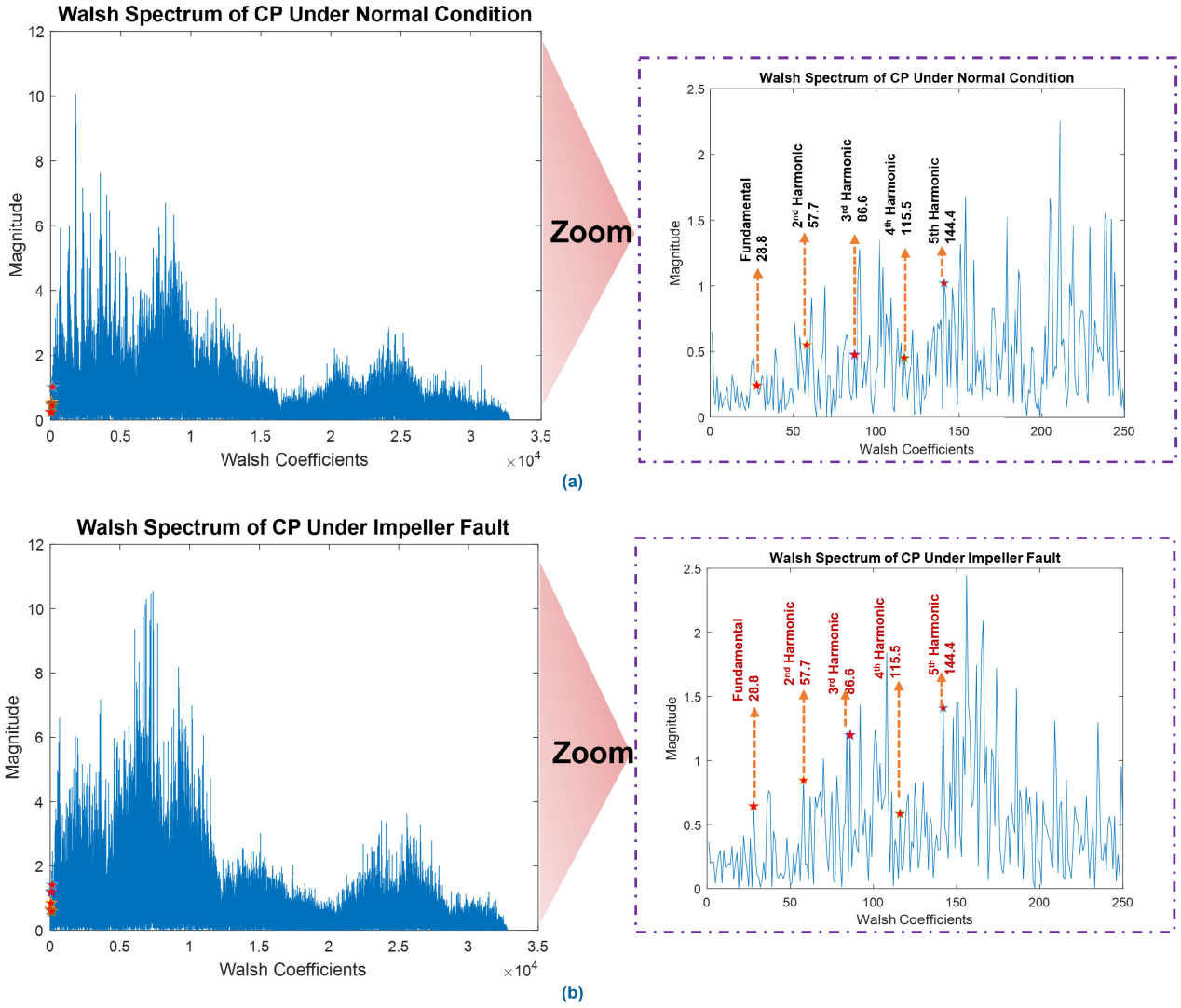


FIGURE 5. Walsh coefficients of the CP (a) Walsh Coefficients of the CP in normal operating Condition (b) Walsh Coefficients of the CP in Impeller defect operating Condition.

feature pool as presented in Eq. (21).

$$I_{F.pool} = \begin{cases} \forall F_i & \text{if } I_{value} > 0, \text{ illustrative feature} \\ else, & \text{less illustrative feature} \end{cases} \tag{21}$$

4. After selecting the illustrative features and creating an illustrative feature pool, the LDA transformation matrices are applied to the illustrative feature pool (explained in 2.2). The illustrative feature pool helps the LDA to reduce the within-class feature scatteredness. Furthermore, the illustrative features also help the LDA to overcome the penalty graph issue for between class separation as the illustrative feature pool contains only features that are highly similar within the class features.

A discriminant reduced dimensional feature space is obtained from the cosine-LDA. The new reduced dimensional feature space obtained from cosine-LDA has a minimum within the class features scatteredness and a maximum between-class distance. The new feature space is classified using the k-nearest neighbor (KNN) for CP condition identification. The KNN classifier is gaining attention because of its low computational complexity and simple architecture. However, the KNN computational complexity is truly dependent on the dimensions of the provided features. For this reason, cosine LDA is used to reduce the feature dimensions based on an improvement in the discriminancy of the features. The results obtained from the proposed method of CP fault diagnosis and its comparisons with other methods are presented in the next section.

V. EXPERIMENTAL RESULTS AND DISCUSSION

The effectiveness of the proposed CP fault diagnosis framework with fault characteristic Walsh coefficient selection is presented along with its industrial application to fault diagnosis.

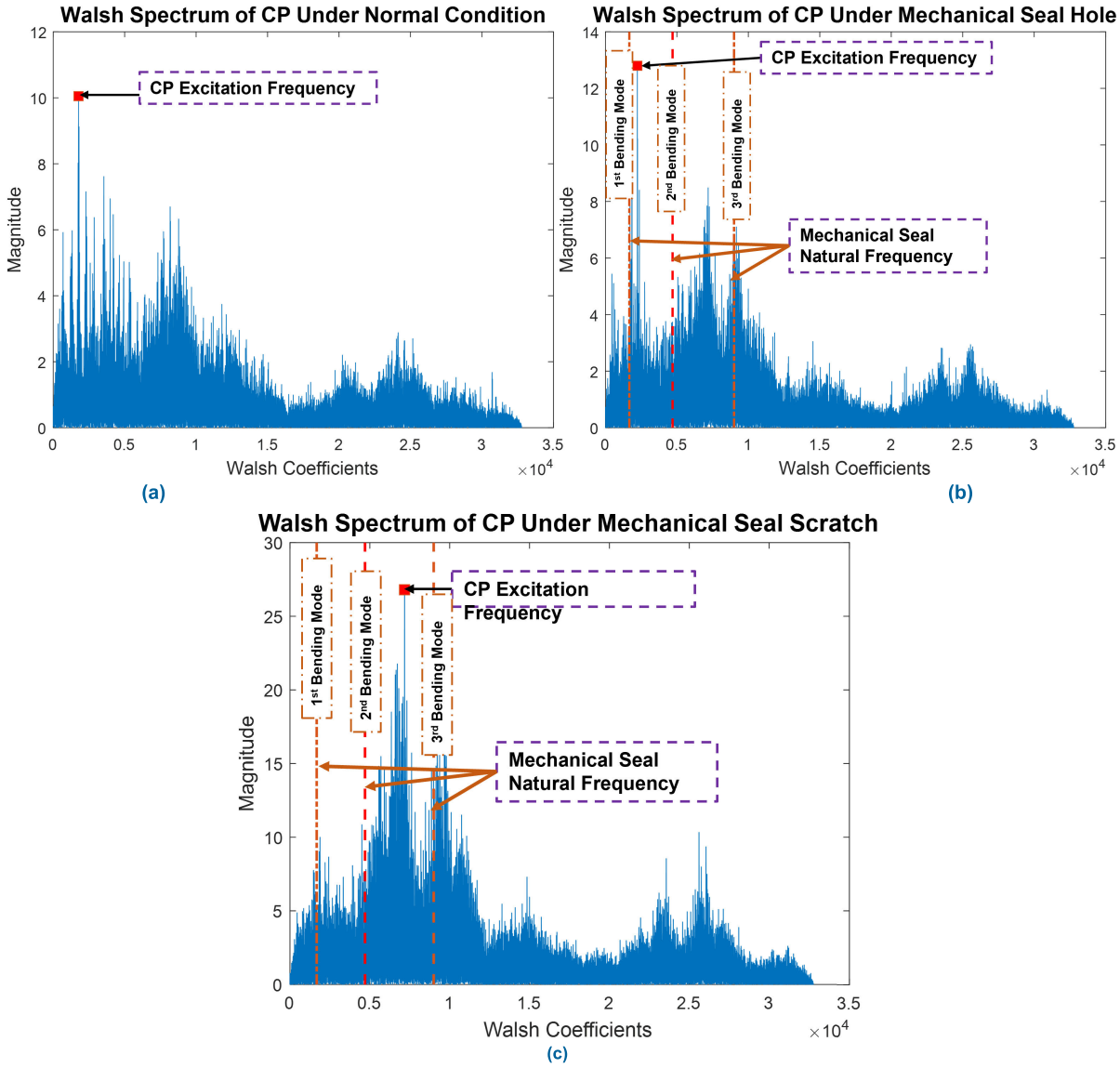


FIGURE 6. Walsh coefficients of the CP under (a) normal operating conditions, (b) MSH defect conditions, (c) MSS defect conditions.

A. VALIDATION OF THE FAULT CHARACTERISTIC WALSH COEFFICIENTS

The proposed method for Walsh coefficients selection is based on the CP FCFs. The CP FCFs were calculated using (13) and (18). For comparison purposes, the Fourier transform of the CP vibration signatures for normal, impeller, and mechanical seal fault conditions is calculated and presented in Figure 7 along with CP FCFs. Figure 7(a) shows that the frequency spectrum of the normal condition of the CP contains the fundamental harmonic and higher harmonic of the impeller imbalance. Furthermore, the amplitude of the fractional harmonics is very small. Figure 5(a) shows that the fundamental harmonic and higher harmonics of the CP impeller imbalance indicate its presence in the Walsh spectrum with smaller amplitude along with fractional harmonics, which are very reasonable for the normal condition of the CP. Figure 7(b) shows the CP vibration spectrum under impeller defect conditions. A very small but noticeable increase in the amplitude of higher harmonics happened. However, the amplitude of the fractional harmonics is very small. Comparing Figure 7(b) and Figure 5(b), we see that the fundamental and higher harmonics are present in the Walsh spectrum, and fractional harmonics are also present in the spectrum that are representing the complex fluid flow interaction with faulty impeller. It is known that mechanical faults in the CP affect the behavior of fundamental and higher harmonics. Therefore, when the change in fundamental and higher harmonics are considered as a sign of impeller fault then it is extremely hard to determine whether the extracted statistical features represent CP impeller defects or the effect of background noise or other mechanical faults. In contrast, Walsh coefficients carry valuable information for impeller

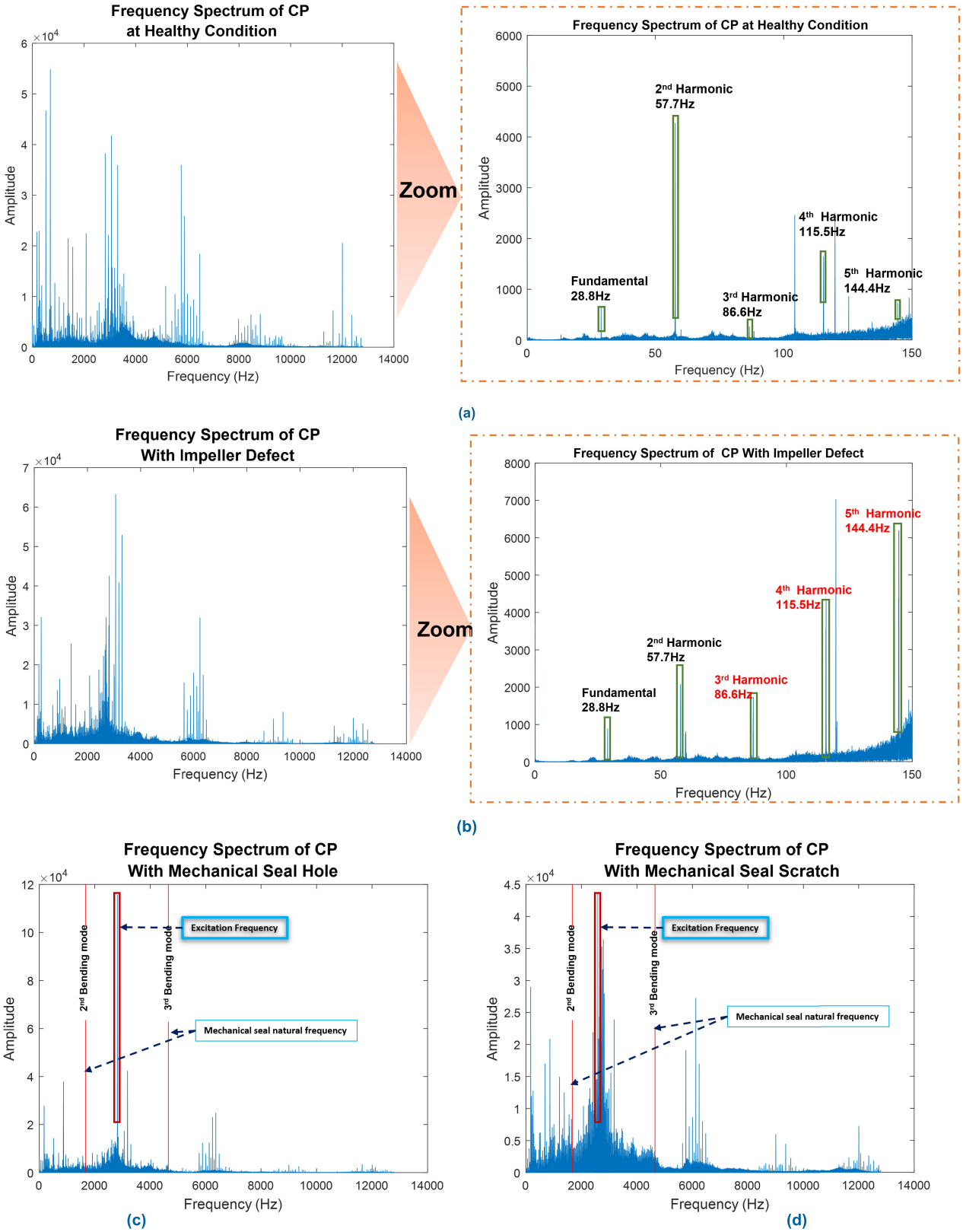


FIGURE 7. Frequency spectrum of the CP under: (a) normal conditions, (b) impeller fault conditions, (c) MSH fault, and (d) MSS fault.

TABLE 1. Performance comparison of the proposed method with the reference methods.

Methods	Results in Percentage%			Average Classification Accuracy
	Macro Precision	Macro Recall	Error Rate	
Proposed	100	100	0	100
Viet et al. [14]	96.3	96.2	7.0	96.20
Tr-LDA [37]	89.6	89.6	16.8	89.56
K-PCA [33]	88.0	87.6	18.1	87.62

defects because fundamental and higher harmonics along with fractional harmonics are present in the Walsh spectrum. Thus, the selected coefficients of the Walsh spectrum can be considered for feature extraction.

In the case of mechanical seal-related faults, the excitation frequency is a valuable feature in the CP spectrum. Figure 7 shows the CP spectrum under MSH and scratch defect conditions. It can be seen from Figure 7(c) and (d) that the CP excitation frequency under MSH and scratch defect conditions occurs between the 2nd and 3rd bending mode of vibration. In contrast, Figure 6 (b) shows the Walsh spectrum of CP under MSH defect condition. Here, the excitation frequency of the CP appeared in between the 1st and 2nd bending MOV with a slight increase in amplitude. For MSS, the excitation frequency of the CP appears between the 2nd and 3rd bending MOV with an increase in the amplitude as can be seen from Figure 6(c). These changes in the coefficient for excitation frequency can be helpful for discriminant feature extraction for CP under mechanical seal defect conditions. Furthermore, the higher coefficients of the Walsh transform, which occurs at the 4th mode or higher MOV may be due to microstructural CP vibration, and these coefficients can be truncated from the Walsh spectrum. As compared to the Fourier spectrum of the CP, the Walsh coefficients of the CP up to 3rd mode of vibration carry enough discriminatory signal level information, and these coefficients can be used for statistical feature extraction.

B. CONFIGURATION OF THE DATASET

In this paper, a 300-second-long signal was acquired from the CP under normal, MSH, MSS, and impeller defect conditions, which results in a total of 1200 signal instances. Statistical features were extracted from these signal instances, resulting in a feature pool consisting of $N_{class} \times N_{signal} \times N_{feature}$, where N_{class} is the CP condition (class), N_{signal} is the signal instance, and $N_{feature}$ is the extracted features.

A K-Fold cross-validation (kCV) strategy was adopted for the validation of the proposed method, where k = 3 for each trial. In the kCV, the feature dataset was divided randomly into k-folds, where a sub fold was used for testing a classifier that is trained on k-1 folds. In this study, 200 samples were randomly selected from each class of the CP for training, and the remaining 100 samples were used for testing the classifier. Therefore, each training set contained a total of 800 samples, while the remaining 400 samples were used for testing purposes.

C. CONFIGURATION PROPOSED METHOD FAULT DIAGNOSIS RESULTS WITH THE NEW COSINE LDA

To evaluate the performance of the proposed method for CP fault diagnosis, a comparison was made with the VS and feature preprocessing method [14], supervised dimensionality reduction technique with trace ratio criteria (Tr-LDA) [37], and kernel-based dimensionality reduction technique (K-PCA) [33]. To ensure a fair evaluation and repeatability in results, each experiment was repeated 10 times with a random combination of testing and training data. Average classification accuracy (CA), macro precision (mP), macro recall (mR), or true positive rate (TPR), and error rate (ER) are the matrices used for comparisons between the proposed method and the reference methods. These metrics for each class were calculated using the formulas below:

$$CA = \frac{1}{n}\sum_{j=1}^{n}\left(\sum_{m=1}^{L}\frac{T_{TP}^{j,m}}{T_{sanples}}\right) \times 100(\%) \tag{22}$$

$$mP = \frac{1}{n}\sum_{j=1}^{n}\left(\frac{(T_{TP}^{j,m})}{T_{TP}^{j,m} + T_{FP}^{j,m}}\right) \times 100(\%) \tag{23}$$

$$TPR_m = \frac{1}{n}\sum_{j=1}^{n}\left(\frac{(T_{TP}^{j,m})}{T_{TP}^{j,m} + T_{FN}^{j,m}}\right) \times 100(\%) \tag{24}$$

$$ER = \frac{1}{n}\sum_{j=1}^{n}\left(\frac{(T_{TP}^{j,m}) + (T_{FN}^{j,m})}{(T_{TP}^{j,m}) + (T_{FN}^{j,m}) + T_{TN}^{j,m} + T_{FP}^{j,m}}\right) \times 100(\%) \tag{25}$$

In (22), (23), (24), and (25) the true positives are represented by $T_{TP}^{j,m}$, the true negatives by $T_{TN}^{j,m}$, the false positives

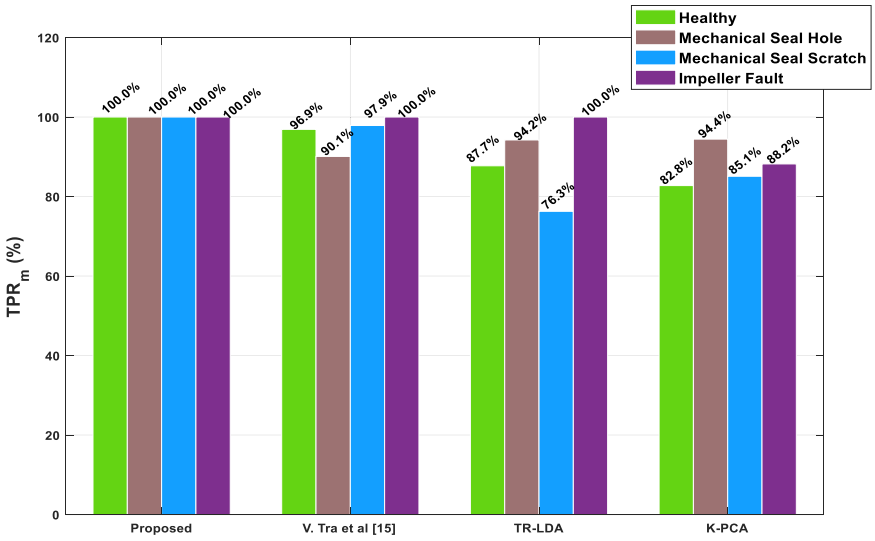


FIGURE 8. True positive rate (TPR) of the proposed method against reference methods for each operating condition of the CP.

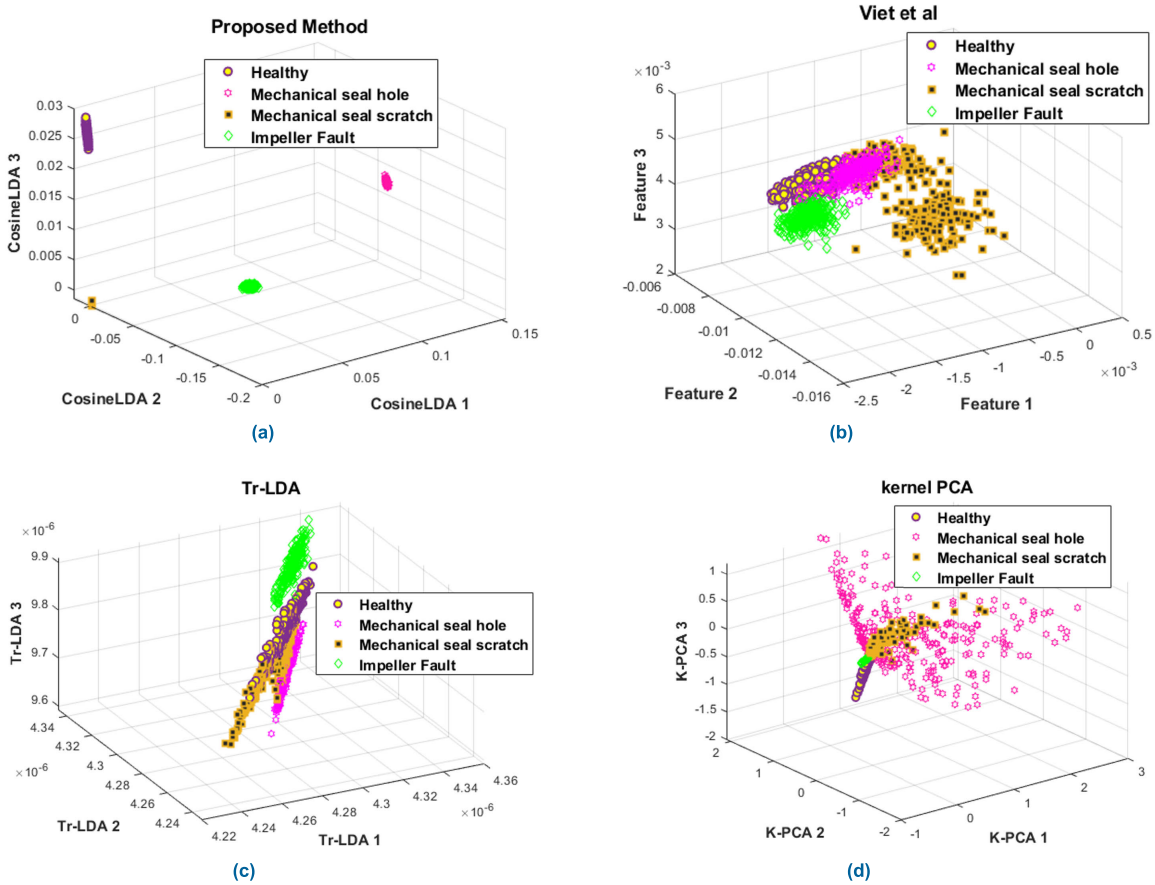


FIGURE 9. Three-dimensional feature space representation (a) Obtained from the proposed method (b) obtained from Tra and Kim [14] (c) obtained from Tr-LDA [37] (d) obtained from K-PCA [33].

by $T_{FP}^{j,m}$, the false negatives by $T_{FN}^{j,m}$, which are classified as class m by the classifier, the iteration of the k folds is represented by j, and the samples in the testing set is $T_{samples}$, where n represents the k folds of the cross-validation.

After applying the proposed method to the CP VS obtained under normal and defective conditions, the proposed method outperformed the reference methods and classified the CP conditions with an average CA of 100%, an mP of 100% with

an ER of 0% as given in Table 1. The TPR for each class is shown in Figure 8.

The results obtained from the proposed method can be explained as follows. MF in the CP results in random variations in the VS. These fluctuations are represented by the FCIs in the CP spectrum. The FCIs occur at lower frequencies and contain little energy. Thus, they are overwhelmed by macrostructural vibration noise. A non-sinusoidal type of transform such as a Walsh transform can mitigate this issue as the high energy impulses occur at lower coefficients. In addition to this, identifying and selecting the fault characteristic coefficient of the Walsh transform is very important as the discriminancy of the statistical features is truly based on the preprocessing of the VS and the raw statistical features. For this reason, the proposed method first selects fault characteristic coefficients of the Walsh transform. After selecting the coefficients, the proposed method extracts 16 statistical features in the time and spectral domain for each CP condition. To obtain discriminant information from the raw feature pool, a new cosine LDA is applied. Cosine LDA chooses highly similar within the class features and adds them to the illustrative feature pool, which contains key discriminant features that represent the condition of the centrifugal pump. To achieve maximum between-classes separation and maintain original class information, LDA is then applied to the illustrative feature pool. As can be observed from Figure 9 (a), the features obtained from the proposed method are highly separable. Furthermore, Figure 9(a) provides strong evidence for the high CA and the effectiveness of the proposed method. The method of Tra and Kim [14] removes the noise from the signal using the BSS technique. To improve the classification accuracy of KNN, that method uses the genetic algorithm for key feature selection from a large feature pool. The large feature pool consists of time, frequency, time-frequency domain features obtained from the preprocessed VS. After applying this method to our experimental setup, we obtained an average CA of 96.20%, an average TPR of 96.2%, and an mP of 96.3% with an ER of 7.0% as given in Table 1. The TPR for each class is shown in Figure 8. The CA of 96.20% was expected because the unimpaired signal in the BSS technique is obtained from a mixing matrix. This unimpaired signal often results in loss of important fault-related information. Furthermore, the fitness function of the genetic algorithm also affects the feature selection process. Despite the drawback, this method can be effective for CP fault diagnosis since the average CA of this method is greater than 95%. Likewise, the average TPR for MSS fault and IF is very close to the proposed method as can be seen from Figure 8. However, in the case of closely varying severity faults (such as normal conditions and a MSH fault), the presented method cannot classify them effectively, which leads the method to a higher ER, as can be seen from Figure 9(b).

Tr-LDA [37] is a linear dimensionality technique that maximizes between classes distance and reduces within the class feature scatteredness using a trace ration criterion with LDA transformation matrices. After implementing the presented method to our experimental setup, we obtained an average CA of 89.56%, an average TPR of 89.6%, and a mP of 89.6% with an ER of 16.8% as given in Table 1. The TPR for each class is shown in Figure 8. The CA of 89.56% is expected because this method did not consider feature preprocessing before applying the LDA transformation. The feature space obtained from the underperformed Tr-LDA is shown in Figure 9(c). The Tr-LDA successfully reduced the within class feature scatteredness but cannot increase the between classes distance, which led to an ER of 16.8%.

Another method is K-PCA [33], which is a modified version of traditional PCA for dimensionality reduction using a kernel function. Rather than computing the covariance matrix, K-PCA computes the principal eigenvectors of the kernel matrix. By implementing the steps provided for K-PCA in [33] for our dataset, we obtained an average CA of 87.6%, an average TPR of 87.6%, and a mP of 88.0% with an ER of 18.1% as given in Table 1. The TPR for each class is shown in Figure 8. The weak performance of K-PCA is expected because of the RBF kernel parameter tuning. Finding the best kernel parameter for K-PCA requires extensive experimentation. From Figure 9(d) it can be observed that the K-PCA cannot discriminate features effectively. Due to weak feature discrimination, we have a classification ER of 18.1% for our dataset.

Overall, the method proposed for CP condition monitoring is very efficient for soft mechanical defect identification and classification. Furthermore, the proposed method is computationally fast and easy to implement. The effectiveness and the fast computation of the proposed method arise from its core idea: CP VS preprocessing and raw statistical feature preprocessing. The computational property, easy implementation, and the results obtained from the proposed CP fault diagnosis strategy make it desirable for industrial use.

VI. CONCLUSION

In this paper, we propose a new fast fault diagnosis strategy for centrifugal pump soft mechanical faults. To obtain vibration signatures of the CP under normal and defective condition, experimental setup was established which is presented in the early part of this paper. To identify the condition of the CP, the proposed method for CP fault diagnosis is divided into three stages. In the first stage, Walsh fault characteristic coefficients were selected. In the second phase, raw statistical features in the time and Walsh spectrum domains were extracted from the selected fault characteristic coefficient of the Walsh transform. In the final step, low dimensional discriminant feature space was obtained using cosine linear discriminant analysis, which selects highly similar interclass features from the raw hybrid statistical feature pool and then reduces the dimension of the selected features using linear discriminant analysis. The reduced dimension discriminant feature space is provided as an input to the K-nearest neighbor classifier for the classification task. The experimental results

obtained from the proposed method reveal that the proposed method is sensitive to soft mechanical faults of a centrifugal pump with closely varying severities and thus outperformed the reference methods with a tested classification accuracy of 100%. It is worth noticing that the proposed method is not tested for hydraulic faults of the centrifugal pump. Moreover, smaller number of features have been considered in this study and, high variance will be an issue if a classification algorithm other than K-NN is applied. All these issues will be considered for future work.

REFERENCES

[1] S. B. Rane and Y. A. M. Narvel, "Re-designing the business organization using disruptive innovations based on blockchain-IoT integrated architecture for improving agility in future industry 4.0," *Benchmarking, Int. J.*, vol. 28, no. 5, pp. 1883–1908, May 2021, doi: 10.1108/BIJ-12-2018-0445.

[2] Y. Jiang, S. Yin, and O. Kaynak, "Performance supervised plant-wide process monitoring in industry 4.0: A roadmap," *IEEE Open J. Ind. Electron. Soc.*, vol. 2, pp. 21–35, 2021, doi: 10.1109/ojies.2020.3046044.

[3] J. S. Rapur and R. Tiwari, "Experimental fault diagnosis for known and unseen operating conditions of centrifugal pumps using MSVM and WPT based analyses," *Measurement*, vol. 147, Dec. 2019, Art. no. 106809, doi: 10.1016/j.measurement.2019.07.037.

[4] S. M. Chittora, *Monitoring of Mechanical Seals in Process Pumps*. Stockholm, Sweden: KTH Royal Institute of Technology, 2018.

[5] G. Mousmoulis, N. Karlsen-Davies, G. Aggidis, I. Anagnostopoulos, and D. Papantonis, "Experimental analysis of cavitation in a centrifugal pump using acoustic emission, vibration measurements and flow visualization," *Eur. J. Mech. B/Fluids*, vol. 75, pp. 300–311, May 2019, doi: 10.1016/j.euromechflu.2018.10.015.

[6] Z. Ahmad, A. E. Prosvirin, J. Kim, and J.-M. Kim, "Multistage centrifugal pump fault diagnosis by selecting fault characteristic modes of vibration and using Pearson linear discriminant analysis," *IEEE Access*, vol. 8, pp. 223030–223040, 2020, doi: 10.1109/ACCESS.2020.3044195.

[7] T. Chen, Z. Wang, X. Yang, and K. Jiang, "A deep capsule neural network with stochastic delta rule for bearing fault diagnosis on raw vibration signals," *Measurement*, vol. 148, Dec. 2019, Art. no. 106857, doi: 10.1016/j.measurement.2019.106857.

[8] N. Lu and T. Yin, "Transferable common feature space mining for fault diagnosis with imbalanced data," *Mech. Syst. Signal Process.*, vol. 156, Jul. 2021, Art. no. 107645, doi: 10.1016/j.ymssp.2021.107645.

[9] S. Cao, Z. Hu, X. Luo, and H. Wang, "Research on fault diagnosis technology of centrifugal pump blade crack based on PCA and GMM," *Measurement*, vol. 173, Mar. 2021, Art. no. 108558, doi: 10.1016/j.measurement.2020.108558.

[10] G. Reges, M. Fontana, M. Ribeiro, T. Silva, O. Abreu, R. Reis, and L. Schnitman, "Electric submersible pump vibration analysis under several operational conditions for vibration fault differential diagnosis," *Ocean Eng.*, vol. 219, Jan. 2021, Art. no. 108249, doi: 10.1016/j.oceaneng.2020.108249.

[11] W. T. Peter, Y. Peng, and R. Yam, "Wavelet analysis and envelope detection for rolling element bearing fault diagnosis-their effectiveness and flexibilities," *J. Vibrat. Acoust.*, vol. 123, no. 3, pp. 303–310, 2001, doi: 10.1115/1.1379745.

[12] H. Sun, S. Yuan, and Y. Luo, "Characterization of cavitation and seal damage during pump operation by vibration and motor current signal spectra," *Proc. Inst. Mech. Eng., A, J. Power Energy*, vol. 233, no. 1, pp. 132–147, Feb. 2019, doi: 10.1177/0957650918769761.

[13] J. Duan, T. Shi, H. Zhou, J. Xuan, and Y. Zhang, "Multiband envelope spectra extraction for fault diagnosis of rolling element bearings," *Sensors*, vol. 18, no. 5, pp. 1–21, 2018, doi: 10.3390/s18051466.

[14] V. Tra and J. Kim, "Pressure vessel diagnosis by eliminating undesired signal sources and incorporating GA-based fault feature evaluation," *IEEE Access*, vol. 8, pp. 134653–134667, 2020, doi: 10.1109/ACCESS.2020.3010871.

[15] J. Antoni, "Fast computation of the kurtogram for the detection of transient faults," *Mech. Syst. Signal Process.*, vol. 21, no. 1, pp. 108–124, 2007, doi: 10.1016/j.ymssp.2005.12.002.

[16] J. Antoni, "The spectral kurtosis: A useful tool for characterising non-stationary signals," *Mech. Syst. Signal Process.*, vol. 20, no. 2, pp. 282–307, Feb. 2006, doi: 10.1016/j.ymssp.2004.09.001.

[17] Y. Jin, C. Shan, Y. Wu, Y. Xia, Y. Zhang, and L. Zeng, "Fault diagnosis of hydraulic seal wear and internal leakage using wavelets and wavelet neural network," *IEEE Trans. Instrum. Meas.*, vol. 68, no. 4, pp. 1026–1034, Aug. 2019, doi: 10.1109/TIM.2018.2863418.

[18] J. Chen, Z. Li, J. Pan, G. Chen, Y. Zi, J. Yuan, B. Chen, and Z. He, "Wavelet transform based on inner product in fault diagnosis of rotating machinery: A review," *Mech. Syst. Signal Process.*, vols. 70–71, pp. 1–35, Mar. 2016, doi: 10.1016/j.ymssp.2015.08.023.

[19] P. Ma, H. Zhang, W. Fan, and C. Wang, "Early fault diagnosis of bearing based on frequency band extraction and improved tunable Q-factor wavelet transform," *Measurement*, vol. 137, pp. 189–202, Apr. 2019, doi: 10.1016/j.measurement.2019.01.036.

[20] A. Wong and X. Y. Wang, "A Bayesian residual transform for signal processing," *IEEE Access*, vol. 3, pp. 709–717, 2015, doi: 10.1109/ACCESS.2015.2437873.

[21] N. E. Huang, Z. Shen, S. R. Long, M. L. Wu, H. H. Shih, Q. Zheng, N. C. Yen, C. C. Tung, and H. H. Liu, "The empirical mode decomposition and the Hubert spectrum for nonlinear and non-stationary time series analysis," *Proc. Roy. Soc. A, Math., Phys. Eng. Sci.*, vol. 454, no. 1971, pp. 903–995, 1998, doi: 10.1098/rspa.1998.0193.

[22] L.-Q. Zuo, H.-M. Sun, Q.-C. Mao, X.-Y. Liu, and R.-S. Jia, "Noise suppression method of microseismic signal based on complementary ensemble empirical mode decomposition and wavelet packet threshold," *IEEE Access*, vol. 7, pp. 176504–176513, 2019, doi: 10.1109/ACCESS.2019.2957877.

[23] X. Xiang, J. Zhou, C. Li, Q. Li, and Z. Luo, "Fault diagnosis based on Walsh transform and rough sets," *Mech. Syst. Signal Process.*, vol. 23, no. 4, pp. 1313–1326, May 2009, doi: 10.1016/j.ymssp.2008.10.004.

[24] M. Maqusi, *Applied Walsh Analysis*. London, U.K.: Heyden & Sons Ltd., 1981. [Online]. Available: https://searchworks.stanford.edu/view/1457859

[25] Q. Gao, H. Tang, J. Xiang, Y. Zhong, S. Ye, and J. Pang, "A Walsh transform-based Teager energy operator demodulation method to detect faults in axial piston pumps," *Measurement*, vol. 134, pp. 293–306, Feb. 2018, doi: 10.1016/j.measurement.2018.10.085.

[26] Z. Ahmad, A. Rai, A. S. Maliuk, and J.-M. Kim, "Discriminant feature extraction for centrifugal pump fault diagnosis," *IEEE Access*, vol. 8, pp. 165512–165528, 2020, doi: 10.1109/access.2020.3022770.

[27] Y. Si, Y. Wang, and D. Zhou, "Key-performance-indicator-related process monitoring based on improved kernel partial least squares," *IEEE Trans. Ind. Electron.*, vol. 68, no. 3, pp. 2626–2636, Mar. 2021, doi: 10.1109/tie.2020.2972472.

[28] M. Cui, Y. Wang, X. Lin, and M. Zhong, "Fault diagnosis of rolling bearings based on an improved stack autoencoder and support vector machine," *IEEE Sensors J.*, vol. 21, no. 4, pp. 4927–4937, Feb. 2021, doi: 10.1109/jsen.2020.3030910.

[29] J. P. S. Gonçalves, F. Fruett, J. G. Dalfré Filho, and M. Giesbrecht, "Faults detection and classification in a centrifugal pump from vibration data using Markov parameters," *Mech. Syst. Signal Process.*, vol. 158, Sep. 2021, Art. no. 107694, doi: 10.1016/j.ymssp.2021.107694.

[30] Y. Lei, *Intelligent Fault Diagnosis and Remaining Useful Life Prediction of Rotating Machinery*. Amsterdam, The Netherlands: Elsevier, 2016.

[31] M. Sohaib, C.-H. Kim, and J.-M. Kim, "A hybrid feature model and deep-learning-based bearing fault diagnosis," *Sensors*, vol. 17, no. 12, p. 2876, Dec. 2017, doi: 10.3390/s17122876.

[32] Z. Xu and J. H. Saleh, "Machine learning for reliability engineering and safety applications: Review of current status and future opportunities," 2020, *arXiv:2008.08221*.

[33] N. R. Sakthivel, B. B. Nair, M. Elangovan, V. Sugumaran, and S. Saravanmurugan, "Comparison of dimensionality reduction techniques for the fault diagnosis of mono block centrifugal pump using vibration signals," *Eng. Sci. Technol., Int. J.*, vol. 17, no. 1, pp. 30–38, Mar. 2014, doi: 10.1016/j.jestch.2014.02.005.

[34] G. Qiu, S. Huang, and Y. Gu, "Experimental investigation and multi-conditions identification method of centrifugal pump using Fisher discriminant ratio and support vector machine," *Adv. Mech. Eng.*, vol. 11, no. 9, 2019, Art. no. 1687814019878041.

[35] L. Yang, X. Liu, F. Nie, and Y. Liu, "Robust and efficient linear discriminant analysis with $L_{2,1}$-norm for feature selection," *IEEE Access*, vol. 8, pp. 44100–44110, 2020, doi: 10.1109/ACCESS.2020.2978287.

[36] H. Wang, S. Yan, D. Xu, X. Tang, and T. Huang, "Trace ratio vs. ratio trace for dimensionality reduction," in *Proc. IEEE Conf. Comput. Vis. Pattern Recognit.*, Jun. 2007, pp. 1–8, doi: 10.1109/CVPR.2007.382983.

[37] X. Jin, M. Zhao, T. W. S. Chow, and M. Pecht, "Motor bearing fault diagnosis using trace ratio linear discriminant analysis," *IEEE Trans. Ind. Electron.*, vol. 61, no. 5, pp. 2441–2451, May 2014, doi: 10.1109/TIE.2013.2273471.
[38] S. Yedidiah, *Centrifugal Pump User's Guidebook: Problems Solutions*. New York, NY, USA: Springer, 2012.
[39] *Condition Monitoring and Diagnostics of Machines—Vibration Condition Monitoring—Part 1: General Procedures*, document ISO 13373-1, 2002. [Online]. Available: https://www.iso.org/standard/21831.html



ZAHOOR AHMAD received the B.S. degree in computer engineering from the COMSATS Institute of Information Technology (CIIT), currently called COMSATS University Islamabad (CUI), Attock, Pakistan, in 2016, and the M.S. degree in electronics and information engineering from Korea Aerospace University (KAU), Goyang, South Korea. He is currently pursuing the Ph.D. degree in computer engineering with the University of Ulsan, South Korea.

He has been a Graduate Research Assistant with the Ulsan Industrial Artificial Intelligence (UIAI) Laboratory, University of Ulsan, since 2019. He worked on the development of advanced algorithms for UAV path planning. His current research interests include artificial intelligence, signal processing, fault diagnosis, vibration-based condition monitoring of industrial machinery, and fault feature extraction.

Mr. Ahmad received the institution's highest price of Gold Medal for a B.S. from CUI, Attock. He was awarded with a fully-funded scholarship for a M.S. degree from a Korean Government Project. His recent awards and honors include the National Research Foundation (NRF) of Korea Research Fellowship Scholarship and the University of Ulsan President Excellence Scholarship for pursuing a Ph.D. Program.



AKHAND RAI received the B.Tech. degree in mechanical engineering from the College of Engineering Roorkee, Roorkee, Uttarakhand, India, in 2010, the M.Tech. degree in mechanical engineering from the Indian Institute of Technology-Banaras Hindu University, Varanasi, Uttar Pradesh, India, in 2012, and the Ph.D. degree in mechanical engineering from the Indian Institute of Technology (IIT) Roorkee, Roorkee, in 2018. He is currently working as a Postdoctoral Professional Researcher with the School of Electrical, Electronics and Computer Engineering, University of Ulsan, Ulsan, South Korea. Prior to joining University of Ulsan, he was a Visiting Assistant Professor with the Thapar Institute of Engineering and Technology, Patiala, Punjab, India. His research interest includes fault diagnosis and of rotating machines.



MD JUNAYED HASAN received the B.Sc. degree in computer engineering from Bangladesh Rural Advancement Committee University (BRACU), Dhaka, Bangladesh, in 2016, and the Ph.D. degree in computer engineering from the University of Ulsan (UoU), Ulsan, Republic of Korea, in 2021. He is currently working as a Data Scientist with the Ulsan Industrial AL Laboratory, Department of Electrical, Electronics, and Computer Engineering, UoU. His research interests include the data-driven fault diagnosis and anomaly detection of complex engineering systems using advanced signal processing, feature engineering, explainable artificial intelligence, and machine learning.

He received the "Best Researcher Award" for three consecutive years (2019–2021) for his outstanding contribution toward the research community from UOU. His awards and honors during his Ph.D. included the National Research Foundation (NRF) of Korea Research Fellowship Scholarship and the Brain Korea Scholarship.



CHEOL HONG KIM received the B.S. degree in computer engineering from Seoul National University, Seoul, South Korea, in 1998, the M.S. degree, in 2000, and the Ph.D. degree in electrical and computer engineering from Seoul National University, in 2006. From December 2005 to January 2007, he worked as a Senior Engineer with Samsung Electronics, South Korea. He also worked as a Professor with Chonnam National University, South Korea, from 2007 to 2020. He is currently working as a Professor with the School of Computer Science and Engineering, Soongsil University, South Korea. His research interests include computer systems, embedded systems, deep learning, fault diagnosis, and low power systems.



JONG-MYON KIM (Member, IEEE) received the B.S. degree in electrical engineering from Myongji University, Yongin, South Korea, in 1995, the M.S. degree in electrical and computer engineering from the University of Florida, Gainesville, FL, USA, in 2000, and the Ph.D. degree in electrical and computer engineering from the Georgia Institute of Technology, Atlanta, GA, USA, in 2005.

He is currently a Professor with the Department of Electrical, Electronics, and Computer Engineering, School of IT Convergence, University of Ulsan, Ulsan, South Korea. His research interests include multimedia-specific processor architecture, fault diagnosis and condition monitoring, parallel processing, and embedded systems.

Dr. Kim is a member of the IEEE Industrial Electronics Society.